CD8+ lymphocytes modulate acute ZIKV viremia, innate antiviral immunity and tissue dissemination in nonhuman primates

Blake Schouest[1,2], Marissa Fahlberg[3], Elizabeth A. Scheef[2], Matthew J. Ward[4], Kyra Headrick[4], Robert V. Blair[5], Margaret H. Gilbert[6], Lara A. Doyle-Meyers[6], Victoria W. Danner[6], Dawn M. Wesson[4], Antonito T. Panganiban[2,7], Nicholas J. Maness[2,7]*

[1]Biomedical Sciences Training Program, Tulane University School of Medicine, New Orleans LA 70112

[2]Division of Microbiology, Tulane National Primate Research Center, Covington LA 70433

[3]Division of Immunology, Tulane National Primate Research Center, Covington LA 70433

[4]School of Public Health and Tropical Medicine, Tulane University, New Orleans LA 70112

[5]Division of Comparative Pathology, Tulane National Primate Research Center, Covington LA 70433

[6]Division of Veterinary Medicine, Tulane National Primate Research Center, Covington LA 70433

[7]Department of Microbiology and Immunology, Tulane University School of Medicine, New Orleans LA 70112

*Corresponding author, Nicholas J Maness, nmaness@tulane.edu

Abstract

The critical importance of CD8+ lymphocytes during chronic viral infection is well established, but their roles in acute ZIKV infection remain incompletely explored. Importantly, antiviral CD8 responses could modulate neurological manifestations that have accompanied recent ZIKV outbreaks. The rhesus macaque model of ZIKV is a particularly valuable tool to understand immune mechanisms of ZIKV control due to similarities in immune function to humans and due to their susceptibility to infection with primary human isolates of the virus. In the present study, we infected four adult male rhesus macaques with ZIKV, two of which had been depleted of CD8+ lymphocytes prior to infection. CD8 depletion resulted in delayed viremia and a near absence of innate immune responses in the blood, demonstrated by a complete lack of neutrophil recruitment to the blood and a striking absence of transcriptional changes in type I interferon response and other key immune genes relative to non-depleted controls during acute infection. Depletion also resulted in differential patterns of monocyte expansion and reduced monocyte activation measured by CD169 expression. Notably, CD8-depleted macaques showed possible evidence of compensatory CD4 T cell responses and persistence of neutralizing antibodies at later timepoints, despite clearance of virus from serum. Neural lesions were also evident in both CD8-depleted animals. One of the depleted animals recovered CD8+ lymphocytes by 21 days post-infection and mounted a high magnitude CD8 T cell response against the virus. The other CD8-depleted animal did not recover CD8+ lymphocytes over the course of the study, and post-mortem histology revealed severe brainstem encephalomalacia as well as enhanced viral dissemination in the semen and seminal vesicle. Together, these data support a potential role for CD8+ lymphocytes in control of ZIKV dissemination and in maintaining immune regulation during acute infection of rhesus macaques.

Introduction

Zika virus (ZIKV) has been a known pathogen for over half a century, but severe manifestations of disease were not directly associated with the virus for most of its history. Although recent outbreaks of ZIKV in the Western hemisphere are notorious for neurological complications including congenital Zika syndrome (CZS) and Guillain-Barré syndrome (GBS), most cases remain asymptomatic, and when symptoms arise, they are usually mild and self-limiting [1]. Differential immune responses to ZIKV infection may dictate the severity of accompanying diseases and underlie clinical outcomes.

As the immunological correlates of protection against ZIKV are beginning to be explored, the CD8 T cell response is emerging as an important frontline mediator of viral control, as is true with other flaviviruses. Less is known about CD4 responses in acute ZIKV infection, although a recent study found that CD4 T cells and IFNγ signaling are indispensable for effective humoral responses to ZIKV in mice [2]. CD8+ lymphocyte depletion, which is a well-established immune manipulation in rhesus macaques [3], is therefore a plausible approach to gauge how the absence of CD8+ cells impacts acute viremia and potentially induces surrogate adaptive responses.

CD8+ lymphocytes, including CD8 T cells and NK cells, are well known mediators of antiviral immunity, but their roles in ZIKV infection and control have only been recently addressed. Studies in mice have demonstrated CD8 T cell responses in ZIKV infection, but ZIKV-associated pathology in these models requires deficiency in type-I interferon (IFN) signaling [4, 5], which is not representative of natural ZIKV infection in humans. This is perhaps an unavoidable caveat, as ZIKV is incapable of antagonizing type-I IFN signaling in mice as it does in humans due to a lack of recognition of murine STAT2 by ZIKV NS5 [2, 6]. Disrupting IFN-I signaling, either genetically or through antibody blockade, is therefore necessary to recapitulate ZIKV neurotropism in mouse models. Importantly, these studies have identified dual protective and deleterious effects of CD8 T cell responses in ZIKV infected animals [4, 6]. While CD8+ lymphocyte infiltration of the CNS appears to reduce viral burden in the brain and spinal cord [5], CD8 influx also simultaneously promotes neural damage and hindlimb paralysis [6]. However, these findings have yet to be replicated in a model sufficiently similar to humans genetically and immunologically. Given the recent development [7] and characterization [8, 9] of a rhesus macaque model for ZIKV, we sought to explore the role of CD8+ lymphocytes in acute ZIKV infection by way of CD8+ lymphocyte depletion.

In the present study, we infected four adult male rhesus macaques, two of which had been previously depleted of CD8+ lymphocytes, with a minimally passaged Brazilian ZIKV strain. The CD8-depleted macaques showed striking virus-response patterns that were not evident in nondepleted macaques, including delayed serum viremia, enhanced viral dissemination to peripheral tissues, and global repression of antiviral gene transcription. CD8-depleted animals also manifested brainstem lesions that were characterized by increased inflammation. Finally, the absence of CD8+ lymphocytes appeared to alter patterns of monocyte expansion and activation and induce possible compensatory CD4 T cell and humoral responses.

Results

Delayed serum viremia and altered leukocyte kinetics

CD8+ lymphocyte depletion commenced 14 days prior to ZIKV infection (Fig 1a), and CD8 T cells were undetectable in both treated animals as early as 11 days prior to ZIKV infection (Fig 1b). Following subcutaneous inoculation with ZIKV, nondepleted animals experienced a rapid spike in serum viremia of

3-4.5 logs at 1 dpi (Fig 1c), consistent with previous reports of ZIKV in rhesus macaques [7, 10]. Strikingly, serum viremia in CD8-depleted macaques was delayed by one day until 2 dpi, when viral RNA was higher than in nondepleted animals (Fig 1c). For the remainder of the study, viral kinetics were similar among all animals, peaking at 3 dpi and dropping to undetectable levels by 10 dpi and beyond (Fig 1c). A previous cohort of female macaques infected with the identical strain of ZIKV demonstrated similar patterns of serum viremia to those observed in nondepleted animals (Fig S1a).

The previous female cohort also showed a remarkably consistent spike in neutrophil-to-lymphocyte ratio (NLR), a biomarker of inflammation [11], at 1 dpi (Fig S1c). This pattern was replicated in nondepleted animals, whereas the NLR in CD8-depleted animals did not elevate the day following infection (Fig 1d), potentially due to a slight decline in neutrophils (Fig S1d) and lymphocytes remaining stagnant in peripheral blood (Fig S1e).

To achieve CD8 depletion, we used an antibody targeting CD8α, which is expressed on both CD8 T cells and NK cells. Thus, both cell populations were depleted in animals receiving antibody treatment. Flow cytometric analysis of NK cells in nondepleted animals revealed proliferation early in infection (Fig 1e). Intriguingly, the CD8-depleted macaque HP17 recovered NK cells and CD8 cells at later timepoints, between 15 and 21 dpi (Figs 1e & 1f).

Quelled antiviral gene expression in whole blood

To further probe innate immune responses, we analyzed antiviral responses in whole blood using a qRT-PCR array of 84 antiviral genes in the rhesus macaque genome. Relative to expression levels pre-infection, nondepleted animals showed striking upregulation of several RIG-I like receptors and type-I interferon (IFN) stimulated genes at 3 dpi, synchronous with peak serum viremia (Fig 2a). The most highly induced genes include the pattern recognition receptors TLR3, RIG-I (DDX58), and MDA5 (IFIH1), as well as the IFN-stimulated genes ISG15, MX1, and OAS2. Induction of these genes at 3 dpi was generally followed by a return to near-baseline expression by 15 dpi. The gene expression profiles of both nondepleted animals were remarkably similar (Fig S2).

In contrast to nondepleted animals, CD8-depleted animals showed an absence of transcriptional responses in whole blood at all timepoints tested (Figs 2a and S2). However, CD86 was an exception to this pattern, which was upregulated at 1, 3, and 15 dpi in GH01 but not in HP17 (Fig S2).

Transcriptional analysis of whole blood revealed the general antiviral milieu in CD8-depleted and nondepleted animals, but the identity of the transcriptionally responding immune cells remained elusive. We suspected ZIKV-infected monocytes to be the main contributors to antiviral signaling owing to their reported susceptibility to infection. However, the absence of a response in CD8-depleted macaques could have been due to the lack of responding NK cells, which may contribute to antiviral signaling given their responsiveness to type-I IFNs [12].

To resolve the source of innate signaling, we separated the PBMCs from a nondepleted animal into CD8+ from CD8- fractions and analyzed the expression of a few antiviral genes that we previously found to be expressed in whole blood. We found similar levels of gene induction among both cell fractions, although expression was slightly higher in the CD8- subset (Fig S3). Additionally, transcription of DDX58 (RIG-I) was almost exclusive to CD8- cells.

To further explore whether ZIKV-infected monocytes contribute to signaling within the CD8- fraction, we cultured macrophages from monocytes in vitro, infected the macrophages with ZIKV, and probed antiviral gene expression using a qRT-PCR array. We found highly overlapping transcriptional patterns to those observed in the whole blood of nondepleted animals at 3 dpi (Fig 2b).

Altered monocyte activation and frequency

The divergent transcriptional patterns in CD8-depleted and nondepleted macaques could have been due to differential monocyte phenotypes, given the susceptibility of monocytes to ZIKV infection [13, 14] and early findings that ZIKV-infected monocytes contribute to antiviral signaling [13]. To interrogate immunophenotypic effects of CD8 depletion, we developed a multicolor flow cytometry panel to track innate and adaptive immune cells over time. The resulting data were highly complex, comprising a variety of surface markers and sampling animals at multiple timepoints and with respect to different treatment groups. To survey general immune responses over time, we used viSNE [15], an adaptation of t-distributed stochastic neighbor embedding (tSNE).

CD8 depletion appeared to affect monocyte activation as measured by CD169 expression. Nondepleted animals showed early activation of monocytes, which peaked at 3 dpi and returned sharply to baseline by 15 dpi (Fig 3a). This pattern was present in all monocyte subsets (Fig S4a-c). In contrast, CD8-depleted animals showed a more prolonged trajectory of monocyte activation, persisting beyond 15 dpi. The activation marker CD69 was also decreased on total monocytes in CD8-depleted animals early in infection (Fig S4d).

CD8 depletion also affected patterns of monocyte abundance. Nonclassical monocytes expanded preferentially in CD8-depleted macaques (Fig 3b), while the same was true of intermediate monocytes in nondepleted animals (Fig 3c). Nondepleted animals also showed expansion of classical monocytes at 1 dpi and then again at necropsy (Fig 3d).

viSNE analysis revealed differential expression of CD95 (Fas) in CD8 depletion, which was found to be significantly increased on nonclassical monocytes in CD8-depleted animals (Fig S4e) and on classical monocytes in GH01 at 10-15 dpi (Fig S4f).

Possible compensatory CD4 and humoral responses

CD8 depletion also promoted differential adaptive immune responses to ZIKV. During infection, nondepleted animals showed activation of effector memory (EM) CD8 cells (Figs 4a & 4b). Meanwhile, CD8-depleted animals showed activation of EM CD4 cells (Figs 4a & 4d), a pattern not seen in nondepleted animals. Linear mixed model (LMM) analysis revealed that CD8 depletion significantly increased CD69 expression on EM CD4 cells (+25.6%, P=0.001949).

To further characterize CD8 responses, we performed intracellular cytokine staining (ICS) of PBMCs stimulated with peptides derived from the ZIKV proteome. Nondepleted macaques showed evidence of CD8 T cell responses, which were co-positive for perforin and IFNγ (Fig 4c). Further supporting CD8 responses in these animals, CD8 T cell frequency increased between 3 and 10 dpi (Fig 1f), which appeared to be driven by expansion of naïve and EM CD8 cells (Figs S5a-b). Intriguingly, the CD8-depleted animal HP17 also mounted a CD8 T cell response at 21 dpi (Fig 4c), soon after this animal recovered CD8 cells (Fig 1f). In all animals with CD8 cells present, CD8 T cell responses were greater at the earlier of the two timepoints tested (Fig 4c).

We also used ICS to explore possible compensatory CD4 responses in CD8-depleted macaques. Both depleted animals showed evidence of antigen-specific Th1 responses at necropsy, characterized by co-positivity for IFNγ and IL-2 (Fig 4e). These responses were also antigen-specific in both macaques, preferential toward ZIKV E and NS1. GH01 exhibited moderate CD4 T cell responses at both timepoints tested (15 and 30 dpi), whereas HP17 showed a robust response at 30 dpi alone. Contrastingly, nondepleted animals showed no appreciable Th1 responses to viral peptides. Further supporting compensatory CD4 responses, CD8-depleted animals showed significantly higher proliferation of naïve CD4 cells (Fig S5e, +3.9% Ki67+ cells, P= 0.005396) and CM CD4 cells (Fig S5f, +4.97%, P= 0.003123) in addition to higher activation of CM CD4 (Fig S5f) EM CD4 cells (Fig 4d, +25.6%, P=0.001949) relative to nondepleted macaques.

To gauge humoral responses to ZIKV, we conducted a plaque reduction neutralization test (PRNT) to quantify neutralizing antibody titers in serum. All animals except JP58 showed evidence of neutralizing antibodies at 7 dpi, the earliest post-infection timepoint tested (Fig 4f). While all animals similarly achieved highly neutralizing titers at 15 dpi, nondepleted animals receded in their antibody concentrations beyond this timepoint. Strikingly, CD8-depleted animals retained high titers until necropsy, a finding consistent with significantly higher rates of B cell proliferation in these animals (Fig 4g, +4.0%, 0.004905).

Enhanced tissue dissemination and neuropathology

Given the maintenance of highly neutralizing antibody titers in CD8-depleted macaques, we suspected that virus might be lingering in the peripheral tissues of these animals. Informed by previous reports of ZIKV tropism in rhesus macaques [16, 17], we searched for viral RNA in lymphoid, reproductive, and neural tissues.

CD8-depleted macaques had significantly higher levels of viral RNA in the mesenteric lymph node relative to nondepleted animals (Fig 5a). Additionally, ZIKV was detectable in the cervical and inguinal lymph nodes of all four animals but was most abundant in the CD8-depleted macaque HP17 (Fig 5a).

Although all animals were negative for virus in the testes and prostate, GH01 manifested a high viral load in semen at 21 dpi (Fig 5c), the final timepoint obtained. ZIKV RNA was also detected in the seminal vesicle of GH01 at necropsy (Fig 5a). HP87 showed a minor amount of virus in the semen at 10 dpi, which was cleared by 15 dpi (Fig 5c).

We found no ZIKV RNA in the neural tissues of any animal (Fig 5a). However, we also probed for ZIKV RNA in cerebrospinal fluid (CSF) to further explore potential neural dissemination. All animals except HP87 harbored virus in the CSF, peaking at 7-10 dpi (Fig 5b), after serum viremia had waned. Notably, the CSF viral loads in depleted macaques were over an order of magnitude greater than in nondepleted animals.

Although ZIKV was not detected in the CNS of any animal, CD8-depleted macaques manifested neural lesions that were not present in nondepleted animals. Most strikingly, the brainstem of GH01 showed an area of severe multifocal to coalescing malacia, characterized by vacuolation, swollen axons, and infiltration by lymphocytes and gitter cells (Fig 5d). Gitter cells are occasionally found within dilated myelin sheaths. Scant brown granular pigment (presumed hemosiderin) and a proliferative cerebral vessel adjacent to the malacia may indicate that the malacia is the result of a vascular event (thromboemboli, infarct, ischemia, etc.).

No gross abnormalities were noted in HP17. However, the sciatic nerve of this animal exhibited mild lymphocytic perivasculitis, and the brainstem contained a localized area of gliosis and dilated myelin sheaths (Fig 5e). A cause for these neural inflammatory lesions was not apparent by histology.

Discussion

Owing to the importance of CD8+ T cells in control of ZIKV in mice [4, 5], our aim was to explore the consistency of these findings in rhesus macaques by way of CD8+ lymphocyte depletion. Importantly, the anti-CD8α monoclonal antibody used for depletion targets not only CD8+ T cells but also NK cells. NK cells are well known regulators of antiviral immunity so any deficiency in host response following treatment with anti-CD8a could indicate that either or both type of cells are important for acute control of ZIKV.

Strikingly, CD8-depleted macaques showed a one-day delay in the establishment of serum viremia, in patent contrast to patterns of ZIKV in rhesus macaques observed by our own group (Fig S1) and others [7]. However, CD8 depletion does not appear to drastically alter viral kinetics, given that all animals exhibited similar viral kinetics at later timepoints. The mechanism underlying delayed serum viremia in the absence of CD8+ lymphocytes remains to be explored. However, monocytes are known hosts of ZIKV in blood [13, 14], and there is crosstalk between NK cells and monocytes, [18] an intercellular interaction that is suspected to modulate transcriptional responses to ZIKV infection [13]. Activation signals from NK cells may induce viral replication in infected monocytes, and the absence of NK cells in CD8-depleted macaques could delay early viremia in these animals. Alternatively, NK cells in pigtail macaques are reportedly permissive to ZIKV early in infection [14], so the absence of this potential host cell may contribute to delayed viral replication.

CD8 depletion also appeared to affect peripheral leukocyte homing in response to ZIKV infection. Neutrophil-to-lymphocyte ratio (NLR) is a biomarker of inflammation [11], and we previously observed a highly consistent pattern of NLR spike 1 day following subcutaneous ZIKV inoculation of rhesus macaques. This pattern was replicated in nondepleted animals but not in those depleted of CD8+ lymphocytes, which was an early indication of potentially altered innate immune responses.

Confirming dysregulated innate responses in context of CD8 depletion, these macaques showed a confounding silence of antiviral signaling in whole blood. This contrasted with standard host transcriptional responses in nondepleted animals, with robust induction of several RIG-I-like receptors (RLRs) and type-I IFN-stimulated genes early in infection, concomitant with peak serum viremia. Importantly, there is precedence for sensing of flaviviruses by RLRs [19].

Although we suspected ZIKV-infected monocytes to be the primary contributors to antiviral gene expression, an important caveat of probing whole blood is that the identity of the transcriptionally responding cell types is unknown. Considering that NK cells are highly responsive to type-I IFN [12] and potential targets of ZIKV [14], the absence of NK cells in CD8-depleted animals could conceivably account for the transcriptional silence in these animals. Active gene induction in purified CD8+ cells from a nondepleted animal indicates that NK cells may indeed contribute to antiviral signaling in whole blood. However, antiviral signaling in the CD8- fraction from this same animal affirms an absence of transcriptional activation in CD8-depleted animals that did not simply result from a lack of NK cells.

Focusing on antiviral signaling in myeloid cells, we found that macrophages infected with ZIKV in vitro showed patterns of transcriptional activation largely overlapping with those observed in nondepleted animals. This suggests that ZIKV infected myeloid cell types, such as monocytes, may be driving antiviral gene induction in blood. Further, transcriptional patterns in nondepleted animals as well as in

cultured macrophages (Fig 3) were remarkably similar to responses previously reported in ZIKV infected primary human fibroblasts [20], supporting uniform transcriptional regulation in ZIKV-infected cells regardless of lineage.

Consistent with a model of monocyte-driven transcriptional responses to ZIKV infection, CD8-depleted and nondepleted macaques also differed in their patterns of monocyte frequency and activation. Strikingly, CD8-depleted macaques showed preferential expansion of nonclassical monocytes, an outcome previously observed in human patients infected with Asian-lineage ZIKV [21]. Infection and expansion of nonclassical monocytes was also previously found to be accompanied by an M2-skewed immunosuppressive phenotype [21], which may account for the absence of antiviral gene induction in CD8-depleted macaques in the present study. Future experiments will explore the possibility of immunosuppressive signaling in these animals.

In contrast with CD8-depleted macaques, nondepleted animals showed expansion of intermediate and classical monocyte subsets. A separate study of ZIKV in human patients in Nicaragua indicated preferential infection of intermediate monocytes [22], which are known to exhibit proinflammatory phenotypes. Preferential infection and expansion of intermediate monocytes in nondepleted animals might have contributed to the elevation of antiviral gene transcription in blood.

CD8 depletion also appeared to affect patterns of monocyte activation, which could have further modulated antiviral signaling. Nondepleted animals showed early activation of monocytes, consistent with recent findings of ZIKV infection in rhesus macaques [16, 23]. In contrast, CD8-depleted animals showed a more prolonged trajectory of monocyte activation, which persisted until later timepoints. CD169 (siglec-1) is a sialic acid-binding lectin known to have important roles in virus capture and transport by myeloid cells [24]. Additionally, CD169+ macrophages are shown to be important in the mounting of CD8 T cell responses in viral infection [25]. Enhanced CD169 expression on monocytes in nondepleted macaques might have promoted CD8 responses in these animals.

Indeed, CD8 T cell responses were evident in nondepleted macaques at earlier timepoints, which is corroborated by expansion of naïve CD8 T cells and activation of EM CD8 T cells. Surprisingly, the CD8-depleted animal HP17 also mounted a CD8 T cell response immediately following recovery of CD8+ lymphocytes, supporting the importance of CD8 responses in acute ZIKV infection. There is precedence for CD8 T cell responses in ZIKV-infected mice [26] and humans [27], which appears to be consistent in the rhesus macaque model.

Meanwhile, CD8-depleted macaques showed evidence of Th1 CD4 responses, which might have been induced to compensate for the absence of cytolytic CD8 activity in these animals. This finding too is consistent with mice, which exhibit Th1 polarization of CD4 cells on ZIKV infection [26]. Given the comparative lack of CD4 response in nondepleted animals, these findings imply that CD8 responses, when intact, are the primary mediators of adaptive cellular immunity against ZIKV; however, Th1 responses may provide important second-line antiviral defense to ZIKV in rhesus macaques.

CD8-depleted macaques also showed possibly enhanced humoral responses relative to nondepleted animals. Humoral immunity is known to mediate protection against ZIKV in rhesus macaques, with neutralizing antibodies detected as early as 7-10 dpi [16], consistent with the present study. Interestingly, CD8-depleted animals showed persistence of neutralizing antibodies until necropsy, despite serum viremia being cleared well before this timepoint. The maintenance of high antibody titers suggested that there might be virus lingering in the peripheral tissues of these animals.

Indeed, viral dissemination appeared more extensive in CD8-depleted macaques by necropsy. Despite the small sample size of the present study, either of the CD8-depleted animals showed a higher level of viral RNA in the semen, seminal vesicle, cervical LN, or inguinal LN relative to nondepleted animals. Further, CD8-depleted macaques showed comparatively higher viral loads in the mesenteric lymph node and CSF. Although a previous report indicated variable tissue dissemination of ZIKV in acutely-infected rhesus macaques [17], it was encouraging to observe similar patterns of viral localization within treatment groups.

Despite the absence of ZIKV RNA in the brain of any animal, both CD8-depleted macaques presented with neural lesions at necropsy that were not evident in nondepleted animals. Although the lesions cannot be directly attributed to ZIKV infection, our observations are consistent with pathological manifestations of ZIKV in mice and humans. The most severe lesion was in the brainstem of GH01, the CD8-depleted animal that never recovered CD8 cells. We noted an extensive region of encephalomalacia which showed evidence of Wallerian degeneration, characterized by swollen axons and infiltration of phagocytic gitter cells. Importantly, similar manifestations have been described in ZIKV infection of human fetal brain tissue [28, 29].

Neural lesions in HP17 were less severe, and interestingly, this animal also recovered CD8 cells and mounted CD8 T cell responses during infection. The sciatic nerve of HP17 exhibited mild inflammation, a location that ZIKV has previously been identified in mice depleted of CD8 cells [4]. Also, the brainstem contained glial nodules, which are an indicator of CNS damage that can be seen in viral encephalitis

Although it is tempting to speculate that CD8 depletion in GH01 and HP17 promoted neural dissemination of ZIKV and consequent pathological sequalae, our inability to detect viral RNA precludes this conclusion. Because the virus was cleared from the CNS within 30 dpi, it is possible that these lesions could still be virus associated even if viral RNA was not detectable in these lesions at the time of necropsy. It is worth noting that CNS localization of ZIKV has been observed as early as 5 dpi in acutely infected macaques [10]. Separately, a recent study of acute ZIKV infection in rhesus macaques failed to identify ZIKV RNA in the CNS at 14 dpi, despite diffuse patterns of viral dissemination [17]. These findings establish precedence for early CNS dissemination of ZIKV in nonhuman primates, which may be cleared later in infection.

In CD8-depleted animals, the absence of NK and CD8 T cell surveillance could have facilitated ZIKV infection of neural tissues, but infection might have been transient due to the eventual priming of CD4 and humoral responses or other immune responses. Additionally, ZIKV is shown to localize as discrete foci in rhesus macaque tissues [23], complicating the detection of sparse viral lesions within organs. The absence of antiviral gene induction and IFN signaling in CD8-depleted macaques could have also contributed to viral dissemination, given that type-I IFN signaling may limit ZIKV neurotropism [6, 31].

In summary, the present study illustrates a pliable dynamic between ZIKV and its hosts. CD8 depletion appears to alter patterns of innate immune activation and regulation, possibly disrupting patterns of antiviral signaling. CD8 T cells may provide default adaptive immune responses to ZIKV, and their absence may induce compensatory CD4 and humoral responses. Finally, CD8+ lymphocytes appear to constitute frontline defenses to ZIKV, potentially limiting viral dissemination to lymphoid tissues, reproductive organs, and the CNS.

Methods

Animal experiments

The four adult male Indian origin rhesus macaques (*Macaca mulatta*) utilized in this study were housed at the Tulane National Primate Research Center (TNPRC). The TNPRC is fully accredited by AAALAC International (Association for the Assessment and Accreditation of Laboratory Animal Care), Animal Welfare Assurance No. A3180-01. Animals were cared for in accordance with the NRC Guide for the Care and Use of Laboratory Animals and the Animal Welfare Act Animal experiments were approved by the Institutional Animal Care and Use Committee of Tulane University (protocol P0367).

Two animals (GH01 and HP17) were depleted of CD8+ lymphocytes by administration of the anti-CD8α antibody MT807R1 (NHP Reagent Resource; https://www.nhpreagents.org) [3]. Four administrations of 5-10 mg/kg were given subcutaneously or intravenously at days 14, 11, 7, and 10 days pre-infection, as per the distributor's protocol. All four animals were subcutaneously infected with 10^4 PFU of a Brazilian ZIKV isolate at 0 dpi (Fig 1a). For data comparison, we included viral loads and CBC data from a previous cohort of 4 non-pregnant female rhesus macaques (CJ89, GA04, HE78, and JD24) that were similarly infected with the same dose of the same Brazilian ZIKV isolate as was used in this study.

Whole blood, CSF, and semen were obtained from animals at the indicated timepoints. Peripheral blood mononuclear cells (PBMCs) were isolated using SepMate tubes (Stemcell Technologies) according to the manufacturer's protocol. At necropsy, the indicated tissues were collected and snap-frozen.

Virus quantification

Viral RNA (vRNA) was extracted from serum and CSF using the High Pure Viral RNA Kit (Roche). Semen, as well as the indicated lymphoid, reproductive, and neural tissues were homogenized in Qiazol (Qiagen) using disposable tissue grinders (Fisherbrand), and RNA was isolated using the RNeasy Lipid Tissue Mini Kit (Qiagen). vRNA from body fluids and tissues was quantified using qRT-PCR as described previously [8].

Antiviral gene expression assays

2.5 ml whole blood was drawn from each animal at 0, 1, 3, and 15 dpi into PAXgene blood RNA tubes (PreAnalytiX) and equilibrated to -80˚C as per the manufacturer's protocol. RNA was extracted from blood samples using the PAXgene blood RNA kit (PreAnalytiX), and cDNA was synthesized using the RT2 First Strand Kit (Qiagen). The rhesus macaque antiviral response was analyzed by way of qRT-PCR using RT2 Profiler PCR Arrays (Qiagen).

To identify cells contributing to antiviral signaling in blood, the CD8 microbead kit (Miltenyi Biotec) was used to separate CD8+ from CD8- fractions in PBMCs from the nondepleted animal JP58 at peak transcriptional activity (3 dpi). RNA was isolated from cell fractions using the RNeasy Mini Kit (Qiagen), and cDNA was synthesized using the RT2 First Strand Kit (Qiagen). RT2 qPCR Primer Assays (Qiagen) were used to analyze expression of ISG15, OAS2, and DDX58 relative to b-actin (ACTB) in CD8+ and CD8- fractions.

To characterize antiviral signaling in myeloid cells, PBMCs were isolated from the whole blood of 4 naïve colony rhesus macaques as described above, and CD14 microbeads (Miltenyi Biotec) were used to isolate monocytes. Monocytes were cultured at 1×10^6 cells/ml in RPMI-1640 medium supplemented with 1% human AB serum (Sigma), 20 ng/ml M-CSF (Peprotech), 1% L-glutamine, and 1% penicillin/streptomycin. After 7 days of culture, monocytes were sufficiently differentiated into

366 macrophages and were infected with the same Brazilian ZIKV isolate described above. At 24 hpi, RNA
367 was extracted using the RNeasy Mini Kit (Qiagen), and qRT-PCR arrays were used to analyze rhesus
368 antiviral signaling as described previously.

369 ## Flow cytometry and gating strategy

370 PBMCs from the indicated timepoints were thawed, washed, and stained using Live/Dead Fixable Aqua
371 Dead Cell Stain Kit (Invitrogen). PBMCs were then stained for the surface markers CD16 (AL488;
372 BioLegend), CD169 (PE; BioLegend), CD28 (PECF594; BD Biosciences), CD95 (PCP-Cy5.5;
373 BioLegend), CD3 (PE-Cy7; BD Biosciences), CD8 (PacBlue; BioLegend), CD14 (BV605; BD
374 Biosciences), HLA-DR (BV650; BioLegend), NKG2A (APC; Beckman Coulter), and CD4 (APC-H7;
375 BD Biosciences). Cells were subsequently fixed in FluoroFix buffer (BioLegend), permeabilized using
376 Perm/Wash buffer (BioLegend), and stained intracellularly for CD69 (BV711; BD Biosciences) and Ki67
377 (AL700; BD Biosciences). Flow cytometry was performed on a BD LSRII instrument and data were
378 analyzed using FlowJo (vX.10.4.2) and viSNE (Cytobank) softwares.

379 Cytometry data were first gated for lymphocytes, singlets, and live cells. NK cells were considered as
380 CD8+/CD16+. CD4 T cells (CD3+/CD4+) and CD8 T cells (CD3+/CD8+) were gated into naïve
381 (CD28+/CD95-), central memory (CD28+/CD95+), and effector memory (CD28-/CD95+) subsets. CD3-
382 cells were divided into B cells (DR+/CD14-/CD16-) and monocytes (classical, CD14++/CD16-;
383 intermediate, CD14+/CD16+; nonclassical, $CD14^{low}$/CD16+). Cell subsets were analyzed with respect to
384 frequency, proliferation (Ki67+) and activation (CD69+ or CD169+).

385 ## Intracellular cytokine staining

386 PBMCs from the indicated timepoints were thawed and rested overnight prior to stimulation with peptide
387 pools comprising ZIKV C, M, E, and NS1 (BEI Resources). On peptide stimulation, cells were also
388 treated with brefeldin A (BioLegend), GolgiStop (BD Biosciences), anti-CD28 (NHP Reagent Reference
389 Program, www.nhpreagents.org/), anti-CD49d (BioLegend), and anti-CD107a (AL700; BD Biosciences).
390 24 hours post-stimulation, cells were stained for the surface markers CD3 (PE-Cy7; BD Biosciences),
391 CD8 (PacBlue; BioLegend), and CD4 (APC-H7; BD Biosciences). Cells were also fixed and
392 permeabilized as described above and stained intracellularly for perforin (FITC; Mabtech), granzyme B
393 (PE; Invitrogen), CD69 (PE-CF594; BD Biosciences), IL-2 (PCP-Cy5.5; BD Biosciences), and IFNγ
394 (AL647; BioLegend). Flow cytometry was performed on a BD LSRII instrument and data were analyzed
395 using FlowJo software (vX.10.4.2).

396 ## Plaque reduction neutralization tests

397 ZIKV PRNTs were conducted according to previously published protocols [32, 33]. Briefly, ZIKV MEX-
398 I-44 isolated in Tapachula, Mexico in 2016 was obtained from The University of Texas Medical Branch,
399 Galveston, TX and cultured to passage 8 in Vero cells. Serum specimens were incubated for one hour at
400 serial dilutions of 1:10, 1:20… 1:320 with previously frozen virus stock of know plaque forming unit
401 (PFU). Samples were then inoculated in duplicate onto a mono-layer of Vero cells grown on 6-well
402 plates and allowed to incubate for an additional hour. Infectious material was then removed and replaced
403 with a 1:1 mixture of Vero media and Avicel® before being incubated for 4 days. To read plaques, the
404 Avicel® layer was fixed with 10% neutral buffered formalin. Finally, the formalin-Avicel® layer was
405 removed and the monolayer was stained with crystal violet, washed with tap water and allowed to dry
406 before plaques were counted manually.

407 Percent reduction in observed plaques and a PRNT90 cutoff were used for interpretation. A PRNT90 titer
408 is the dilution of a sample at which a 90% reduction in possible plaques is observed. The maximum

number of potential plaques was obtained for each run using a corresponding back-titration and a linear model was fit to the observed number of plaques for each dilution. A PRNT90 titer was derived for each sample using the linear model and the equation for a straight line in the statistical program R [34]. For samples that were positive but above the resolution of the PRNT assay the value of the greatest number of possible plaques for that run, as determined by the back titration, was assigned for each dilution for use with the linear model.

Histology

Tissues samples collected at necropsy were fixed in Z-Fix (Anatech), embedded in paraffin and 5 μ m thick sections were cut, adhered to charged glass slides, and either stained routinely with hematoxylin and eosin or Prussian blue.

Statistical analysis

For viral loads, Mann-Whitney U tests were performed using GraphPad Prism v6.07 (GraphPad Software). For immune cell phenotyping, linear mixed model analyses were performed using R statistical computing [34] with the *lme4* package [35]. Animal variation was considered a random effect, while fixed effects included CD8 depletion, dpi, and expression level of the marker in question. P-values were calculated using likelihood ratio tests of the full model against a reduced model lacking the effect of CD8 depletion.

Figure legends

Fig 1

Delayed serum viremia and altered leukocyte kinetics in CD8-depleted macaques. (**A**) Study design; of the 4 adult male rhesus macaques used in the study, 2 (GH01 and HP17) were depleted of CD8+ lymphocytes, while the other 2 animals (HP87 and JP58) were not. All animals were infected with a Brazilian isolate of ZIKV, and viremia was tracked over 30 days. (**B**) Total CD8 T cell counts in blood, as determined by flow cytometry. (**C**) Viral RNA in serum over infection. (**D**) Neutrophil-to-lymphocyte ratio (NLR), derived using total neutrophil and lymphocyte counts in blood from complete blood count data. (**E**) NK cell proliferation, as measured by Ki67 expression over time. (**F**) Frequency of CD8 T cells over the course of the study.

Fig 2

Quelled antiviral gene expression in whole blood of CD8-depleted macaques. (**A**) Quantification of antiviral gene transcription in whole blood of nondepleted and CD8-depleted animals, using a qRT-PCR array of 84 genes in the rhesus macaque genome. Fold regulation at 1, 3, and 15 dpi was determined relative to day 0. (**B**) Comparison of antiviral signaling in cultured ZIKV-infected macrophages and the whole blood of nondepleted animals at 3 dpi.

Fig 3

Altered patterns of monocyte activation and frequency in CD8-depleted macaques. (**A**) viSNE analysis of monocyte activation, as measured by CD169 expression. The viSNE clustering profile of monocyte subsets (*left*) and corresponding CD169 heatmaps in nondepleted and CD8-depleted macaques over time (*center*), with line graph summary (*right*). (**B-D**) Frequencies of nonclassical (B), intermediate (C), and classical (D) monocyte subsets over infection.

Fig 4

Possible compensatory CD4 and humoral responses in CD8-depleted macaques. (**A**) viSNE analysis of T cell activation, as measured by CD69 expression. The viSNE clustering profile of CD4 and CD8 T cell subsets (*left*) and corresponding CD69 heatmaps in nondepleted and CD8-depleted macaques over infection (*right*). Circled populations indicate effector memory (EM) CD8 cells in nondepleted animals and EM CD4 cells in CD8-depleted animals. (**B**) Kinetics of EM CD8 activation, as measured by CD69 expression. (**C**) CD8 T cell responses, as determined by intracellular cytokine staining (ICS) of PBMCs stimulated with viral peptides derived from the indicated ZIKV proteins. CD8 T cell responses were identified by co-positivity for perforin and IFNγ. (**D**) Kinetics of EM CD4 activation, as measured by CD69 expression. Linear mixed model (LMM) analysis: $P = 0.001949$. (**E**) Th1 responses, determined by ICS for IL-2 and IFNγ. *Inset*: representative antigen-specific cytometry plots for HP17 at 30 dpi. (**F**) Neutralizing antibody titers in serum, represented as PRNT90. (**G**) Kinetics of B cell proliferation, measured by Ki67 expression. LMM analysis: $P = 0.004905$.

Fig 5

Enhanced viral dissemination and neuropathology in CD8-depleted macaques. (**A-C**) Viral loads in lymphatic, neural, reproductive tissues (A), CSF (B), and semen (C). (**D**) GH01 brainstem encephalomalacia. *Top left* and *top right*: area of encephalomalacia (dotted region). Adjacent to the area of malacia a cerebral vessel exhibits medial thickening (arrow). *Bottom left* and *bottom right*: within the area of malacia, swollen axons (spheroids, arrowhead) are seen within dilated myelin sheathes. In some myelin sheaths, axons are absent with infiltration by gitter cells (digestion chamber formation, asterisks). Gitter cells occasionally contain golden brown cytoplasmic pigment (arrow). (**E**) HP17 sciatic nerve and brainstem lesions. *Top left*: small vessels within the sciatic nerve are surrounded by low numbers of lymphocytes (arrows). H&E, 40x, bar = 20 um. *Top right*: a focal glial nodule is present within the gray matter of the brainstem (arrow). H&E, 10x, bar = 100 um. *Bottom left*: there is dilation of adjacent myelin sheaths and spheroid formation (arrowhead). H&E, 20x, bar = 50 um. *Bottom right*: zoom in from bottom left. H&E, 40x, =20 um.

Fig S1

Comparison of viral loads and CBC data to previous female cohort. Data from previous cohort is shown in gray, and data from the present study is overlaid. (**A**) Viral RNA in serum over infection. (**B**) Viral loads in CSF. (**C**) NLR, derived using total neutrophil and lymphocyte counts in blood from CBC data. (**D**) Characteristic spike of neutrophils in nondepleted animals at 1 dpi. (**E**) Characteristic reduction of circulating lymphocytes in nondepleted animals at 1 dpi.

Fig S2

Animal-specific transcriptional responses. Patterns of antiviral gene induction in whole blood at 1, 3, and 15 dpi are represented for each animal individually.

Fig S3

Comparison of antiviral gene expression in CD8+ and CD8- fractions of PBMC. Induction of the antiviral genes ISG15, OAS2, and DDX58 was analyzed in sorted CD8+ and CD8- fractions of PBMCs from a nondepleted animal at peak transcriptional activity. Graph indicates fold regulation relative to b-actin.

Fig S4

Modulation of monocyte phenotype by CD8 depletion. (**A-C**) Kinetics of monocyte activation, as measured by CD169 expression in classical (A), intermediate (B), and nonclassical (C) subsets. (**D**) Overall monocyte activation, as measured by CD69 expression. (**E-F**) Kinetics of monocyte CD95 MFI in nonclassical (E) and classical (F) subsets.

Fig S5

Adaptive immune cell immunophenotyping. (**A**) Frequencies of EM, central memory (CM), and naïve CD8 subsets over infection. (**B**) Naïve CD8 cell activation (DR+) and proliferation (Ki67+). (**C**) Kinetics of CD8α MFI in total CD8 cells. (**D**) Frequencies of EM, CM, and naïve CD4 subsets over infection. (**E**) Naïve CD4 cell activation (DR+) and proliferation (Ki67+). For Ki67 expression, LMM analysis: $P = 0.005396$. (**F**) CM CD4 cell activation (DR+) and proliferation (Ki67+). LMM analysis of Ki67: $P = 0.003123$. (**G**) Frequencies of total CD4 T cells over infection.

Bibliography

1. Plourde AR, Bloch EM. A Literature Review of Zika Virus. Emerg Infect Dis. 2016;22(7):1185-92. Epub 2016/04/14. doi: 10.3201/eid2207.151990. PubMed PMID: 27070380; PubMed Central PMCID: PMCPMC4918175.

2. Lucas CGO, Kitoko JZ, Ferreira FM, Suzart VG, Papa MP, Coelho SVA, et al. Critical role of CD4+ T cells and IFNγ signaling in antibody-mediated resistance to Zika virus infection. Nat Commun. 2018;9. doi: 10.1038/s41467-018-05519-4. PubMed PMID: 30087337; PubMed Central PMCID: PMCPMC6081430.

3. Schmitz JE, Simon MA, Kuroda MJ, Lifton MA, Ollert MW, Vogel CW, et al. A nonhuman primate model for the selective elimination of CD8+ lymphocytes using a mouse-human chimeric monoclonal antibody. Am J Pathol. 1999;154(6):1923-32. doi: 10.1016/S0002-9440(10)65450-8. PubMed PMID: 10362819; PubMed Central PMCID: PMCPMC1866630.

4. Elong Ngono A, Vizcarra EA, Tang WW, Sheets N, Joo Y, Kim K, et al. Mapping and Role of the CD8(+) T Cell Response During Primary Zika Virus Infection in Mice. Cell Host Microbe. 2017;21(1):35-46. Epub 2017/01/13. doi: 10.1016/j.chom.2016.12.010. PubMed PMID: 28081442; PubMed Central PMCID: PMCPMC5234855.

5. Huang H, Li S, Zhang Y, Han X, Jia B, Liu H, et al. CD8+ T Cell Immune Response in Immunocompetent Mice during Zika Virus Infection. J Virol. 2017;91(22). doi: 10.1128/jvi.00900-17. PubMed PMID: 28835502; PubMed Central PMCID: PMCPMC5660488.

6. Jurado KA, Yockey LJ, Wong PW, Lee S, Huttner AJ, Iwasaki A. Antiviral CD8 T cells induce Zika-virus-associated paralysis in mice. Nat Microbiol. 2018;3(2):141-7. Epub 2017/11/20. doi: 10.1038/s41564-017-0060-z. PubMed PMID: 29158604; PubMed Central PMCID: PMCPMC5780207.

7. Dudley DM, Aliota MT, Mohr EL, Weiler AM, Lehrer-Brey G, Weisgrau KL, et al. A rhesus macaque model of Asian-lineage Zika virus infection. Nat Commun. 2016;7:12204. Epub 2016/06/28. doi: 10.1038/ncomms12204. PubMed PMID: 27352279; PubMed Central PMCID: PMCPMC4931337.

8. Magnani DM, Rogers TF, Maness NJ, Grubaugh ND, Beutler N, Bailey VK, et al. Fetal demise and failed antibody therapy during Zika virus infection of pregnant macaques. Nat Commun. 2018;9(1):1624. Epub 2018/04/24. doi: 10.1038/s41467-018-04056-4. PubMed PMID: 29691387; PubMed Central PMCID: PMCPMC5915455.

9. Best K, Guedj J, Madelain V, de Lamballerie X, Lim SY, Osuna CE, et al. Zika plasma viral dynamics in nonhuman primates provides insights into early infection and antiviral strategies. Proc Natl Acad Sci U

S A. 2017;114(33):8847-52. Epub 2017/08/01. doi: 10.1073/pnas.1704011114. PubMed PMID: 28765371; PubMed Central PMCID: PMCPMC5565429.

10. Osuna CE, Lim SY, Deleage C, Griffin BD, Stein D, Schroeder LT, et al. Zika viral dynamics and shedding in rhesus and cynomolgus macaques. Nat Med. 2016;22(12):1448-55. Epub 2016/10/03. doi: 10.1038/nm.4206. PubMed PMID: 27694931; PubMed Central PMCID: PMCPMC5293594.

11. Gao Y, Wang WJ, Zhi Q, Shen M, Jiang M, Bian X, et al. Neutrophil/lymphocyte ratio is a more sensitive systemic inflammatory response biomarker than platelet/lymphocyte ratio in the prognosis evaluation of unresectable pancreatic cancer. Oncotarget. 2017;8(51):88835-44. Epub 2017/09/27. doi: 10.18632/oncotarget.21340. PubMed PMID: 29179480; PubMed Central PMCID: PMCPMC5687650.

12. Martinez J, Huang X, Yang Y. Direct action of type I IFN on NK cells is required for their activation in response to vaccinia viral infection in vivo. J Immunol. 2008;180(3):1592-7. PubMed PMID: 18209055.

13. Lum FM, Lee D, Chua TK, Tan JJL, Lee CYP, Liu X, et al. Zika Virus Infection Preferentially Counterbalances Human Peripheral Monocyte and/or NK Cell Activity. mSphere. 2018;3(2). Epub 2018/03/28. doi: 10.1128/mSphereDirect.00120-18. PubMed PMID: 29600283; PubMed Central PMCID: PMCPMC5874443.

14. O'Connor MA, Tisoncik-Go J, Lewis TB, Miller CJ, Bratt D, Moats CR, et al. Early cellular innate immune responses drive Zika viral persistence and tissue tropism in pigtail macaques. Nat Commun. 2018;9(1):3371. Epub 2018/08/22. doi: 10.1038/s41467-018-05826-w. PubMed PMID: 30135445; PubMed Central PMCID: PMCPMC6105614.

15. Amir e-A, Davis KL, Tadmor MD, Simonds EF, Levine JH, Bendall SC, et al. viSNE enables visualization of high dimensional single-cell data and reveals phenotypic heterogeneity of leukemia. Nat Biotechnol. 2013;31(6):545-52. Epub 2013/05/19. doi: 10.1038/nbt.2594. PubMed PMID: 23685480; PubMed Central PMCID: PMCPMC4076922.

16. Hirsch AJ, Smith JL, Haese NN, Broeckel RM, Parkins CJ, Kreklywich C, et al. Zika Virus infection of rhesus macaques leads to viral persistence in multiple tissues. PLoS Pathog. 2017;13(3):e1006219. Epub 2017/03/09. doi: 10.1371/journal.ppat.1006219. PubMed PMID: 28278237; PubMed Central PMCID: PMCPMC5344528.

17. Coffey LL, Pesavento PA, Keesler RI, Singapuri A, Watanabe J, Watanabe R, et al. Zika Virus Tissue and Blood Compartmentalization in Acute Infection of Rhesus Macaques. PLoS One. 2017;12(1):e0171148. Epub 2017/01/31. doi: 10.1371/journal.pone.0171148. PubMed PMID: 28141843; PubMed Central PMCID: PMCPMC5283740.

18. Michel T, Hentges F, Zimmer J. Consequences of the crosstalk between monocytes/macrophages and natural killer cells. Front Immunol. 2012;3:403. Epub 2013/01/04. doi: 10.3389/fimmu.2012.00403. PubMed PMID: 23316194; PubMed Central PMCID: PMCPMC3539656.

19. Muñoz-Jordán JL, Fredericksen BL. How flaviviruses activate and suppress the interferon response. Viruses. 2010;2(2):676-91. Epub 2010/02/23. doi: 10.3390/v2020676. PubMed PMID: 21994652; PubMed Central PMCID: PMCPMC3185611.

20. Hamel R, Dejarnac O, Wichit S, Ekchariyawat P, Neyret A, Luplertlop N, et al. Biology of Zika Virus Infection in Human Skin Cells. J Virol. 2015;89(17):8880-96. Epub 2015/06/17. doi: 10.1128/JVI.00354-15. PubMed PMID: 26085147; PubMed Central PMCID: PMCPMC4524089.

21. Foo SS, Chen W, Chan Y, Bowman JW, Chang LC, Choi Y, et al. Asian Zika virus strains target CD14+ blood monocytes and induce M2-skewed immunosuppression during pregnancy. Nat Microbiol. 2017;2(11):1558-70. doi: 10.1038/s41564-017-0016-3. PubMed PMID: 28827581; PubMed Central PMCID: PMCPMC5678934.

22. Michlmayr D, Andrade P, Gonzalez K, Balmaseda A, Harris E. CD14+CD16+ monocytes are the main target of Zika virus infection in peripheral blood mononuclear cells in a paediatric study in Nicaragua. Nat Microbiol. 2017;2(11):1462-70. doi: 10.1038/s41564-017-0035-0. PubMed PMID: 28970482; PubMed Central PMCID: PMCPMC5997390.

578 23. Hirsch AJ, Roberts VHJ, Grigsby PL, Haese N, Schabel MC, Wang X, et al. Zika virus infection in
579 pregnant rhesus macaques causes placental dysfunction and immunopathology. Nat Commun.
580 2018;9(1):263. Epub 2018/01/17. doi: 10.1038/s41467-017-02499-9. PubMed PMID: 29343712; PubMed
581 Central PMCID: PMCPMC5772047.
582 24. Sewald X, Ladinsky MS, Uchil PD, Beloor J, Pi R, Herrmann C, et al. Retroviruses use CD169-
583 mediated trans-infection of permissive lymphocytes to establish infection. Science. 2015;350(6260):563-
584 7. Epub 2015/10/01. doi: 10.1126/science.aab2749. PubMed PMID: 26429886; PubMed Central PMCID:
585 PMCPMC4651917.
586 25. van Dinther D, Veninga H, Iborra S, Borg EGF, Hoogterp L, Olesek K, et al. Functional CD169 on
587 Macrophages Mediates Interaction with Dendritic Cells for CD8. Cell Rep. 2018;22(6):1484-95. doi:
588 10.1016/j.celrep.2018.01.021. PubMed PMID: 29425504.
589 26. Pardy RD, Rajah MM, Condotta SA, Taylor NG, Sagan SM, Richer MJ. Analysis of the T Cell
590 Response to Zika Virus and Identification of a Novel CD8+ T Cell Epitope in Immunocompetent Mice.
591 PLoS Pathog. 2017;13(2):e1006184. Epub 2017/02/23. doi: 10.1371/journal.ppat.1006184. PubMed
592 PMID: 28231312; PubMed Central PMCID: PMCPMC5322871.
593 27. Grifoni A, Pham J, Sidney J, O'Rourke PH, Paul S, Peters B, et al. Prior Dengue virus exposure
594 shapes T cell immunity to Zika virus in humans. J Virol. 2017. Epub 2017/10/04. doi: 10.1128/JVI.01469-
595 17. PubMed PMID: 28978707; PubMed Central PMCID: PMCPMC5709580.
596 28. Vesnaver TV, Tul N, Mehrabi S, Parissone F, Štrafela P, Mlakar J, et al. Zika virus associated
597 microcephaly/micrencephaly-fetal brain imaging in comparison with neuropathology. BJOG.
598 2017;124(3):521-5. Epub 2016/11/24. doi: 10.1111/1471-0528.14423. PubMed PMID: 27885789.
599 29. Driggers RW, Ho CY, Korhonen EM, Kuivanen S, Jääskeläinen AJ, Smura T, et al. Zika Virus
600 Infection with Prolonged Maternal Viremia and Fetal Brain Abnormalities. N Engl J Med.
601 2016;374(22):2142-51. Epub 2016/03/30. doi: 10.1056/NEJMoa1601824. PubMed PMID: 27028667.
602 30. Garman RH. Histology of the central nervous system. Toxicol Pathol. 2011;39(1):22-35. Epub
603 2010/11/30. doi: 10.1177/0192623310389621. PubMed PMID: 21119051.
604 31. Cumberworth SL, Barrie JA, Cunningham ME, de Figueiredo DPG, Schultz V, Wilder-Smith AJ, et
605 al. Zika virus tropism and interactions in myelinating neural cell cultures: CNS cells and myelin are
606 preferentially affected. Acta Neuropathol Commun. 2017;5(1):50. Epub 2017/06/23. doi:
607 10.1186/s40478-017-0450-8. PubMed PMID: 28645311; PubMed Central PMCID: PMCPMC5481922.
608 32. Lieberman MM, Nerurkar VR, Luo H, Cropp B, Carrion R, de la Garza M, et al. Immunogenicity
609 and protective efficacy of a recombinant subunit West Nile virus vaccine in rhesus monkeys. Clin Vaccine
610 Immunol. 2009;16(9):1332-7. Epub 2009/07/29. doi: 10.1128/CVI.00119-09. PubMed PMID: 19641099;
611 PubMed Central PMCID: PMCPMC2745014.
612 33. Ward MJ, Alger J, Berrueta M, Bock H, Buekens P, Cafferata ML, et al. Zika Virus and the World
613 Health Organization Criteria for Determining Recent Infection Using Plaque Reduction Neutralization
614 Testing. Am J Trop Med Hyg. 2018;99(3):780-2. Epub 2018/06/21. doi: 10.4269/ajtmh.18-0237. PubMed
615 PMID: 29943723.
616 34. R Core Team. R: A language and environment for statistical computing. Vienna, Austria: R
617 Foundation for Statistical Computing; 2018.
618 35. Bates D, Maechler M, Bolker B, Walker S. Fitting Linear Mixed-Effects Models Using lme4.
619 Journal of Statistical Software; 2015.

620

Figure 1: Delayed serum viremia and altered leukocyte kinetics in CD8-depleted macaques

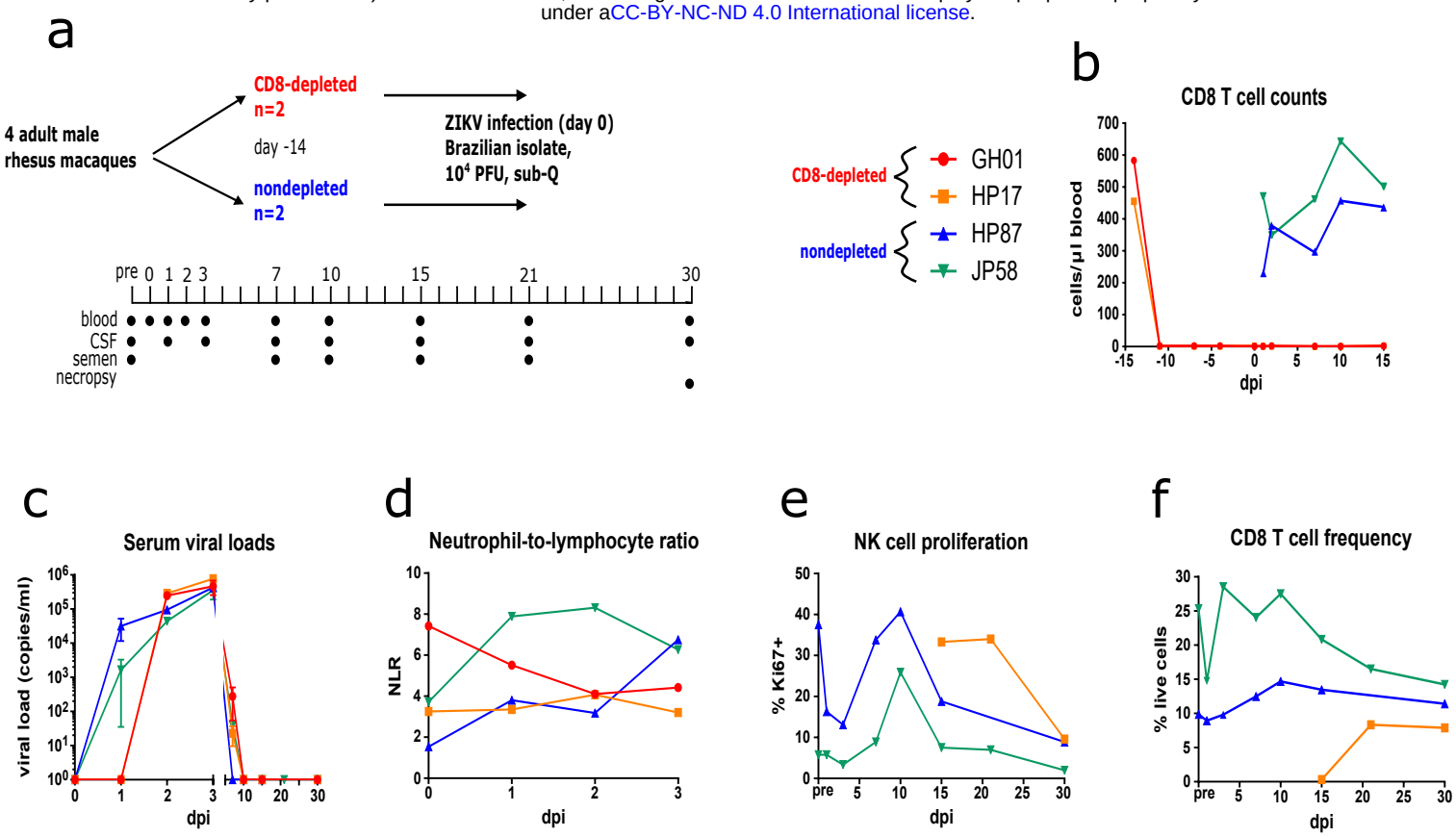

Fig 2: Quelled antiviral gene expression in whole blood of CD8-depleted macaques

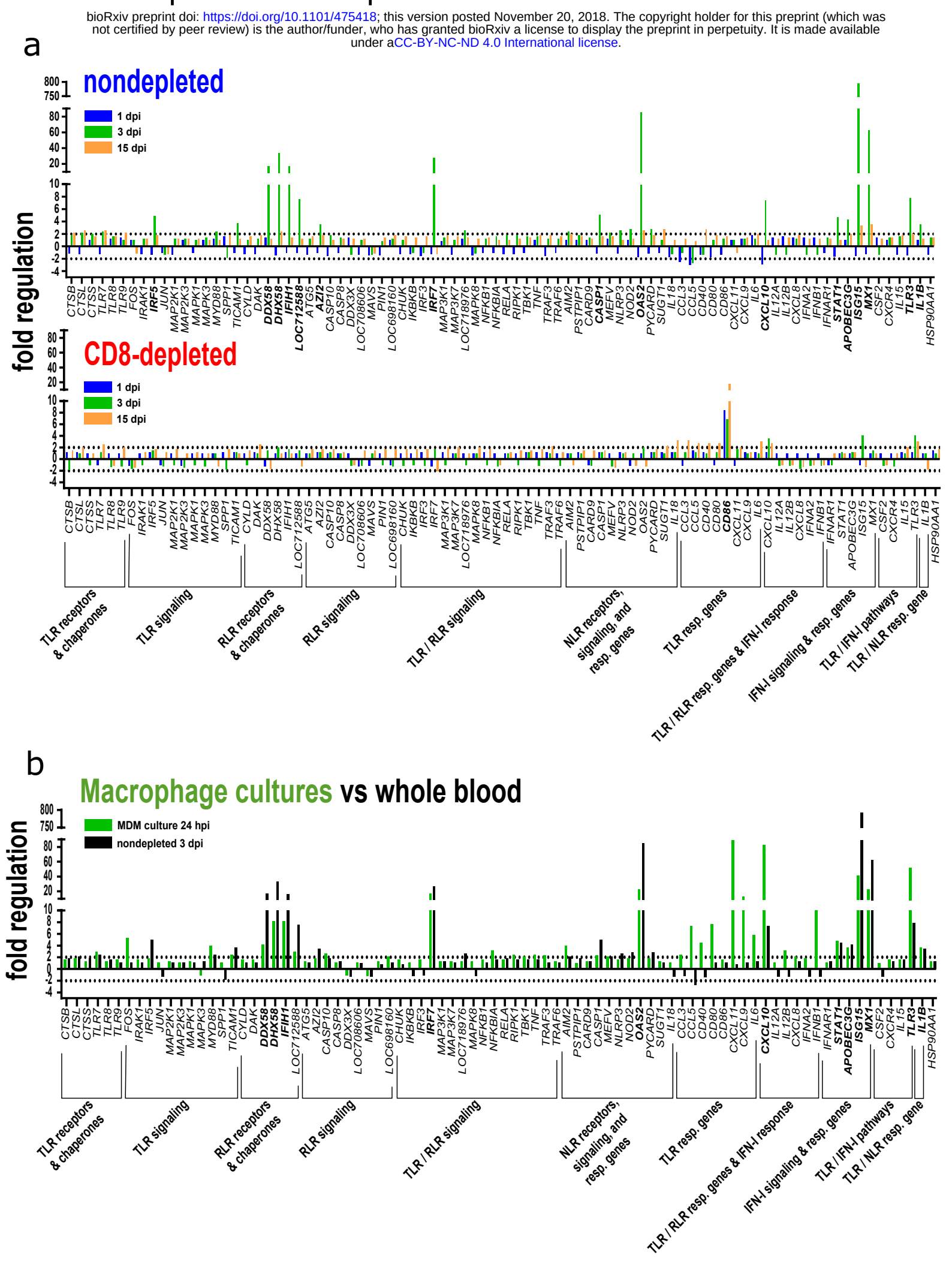

Fig 3: Altered patterns of monocyte activation and frequency in CD8-depleted macaques

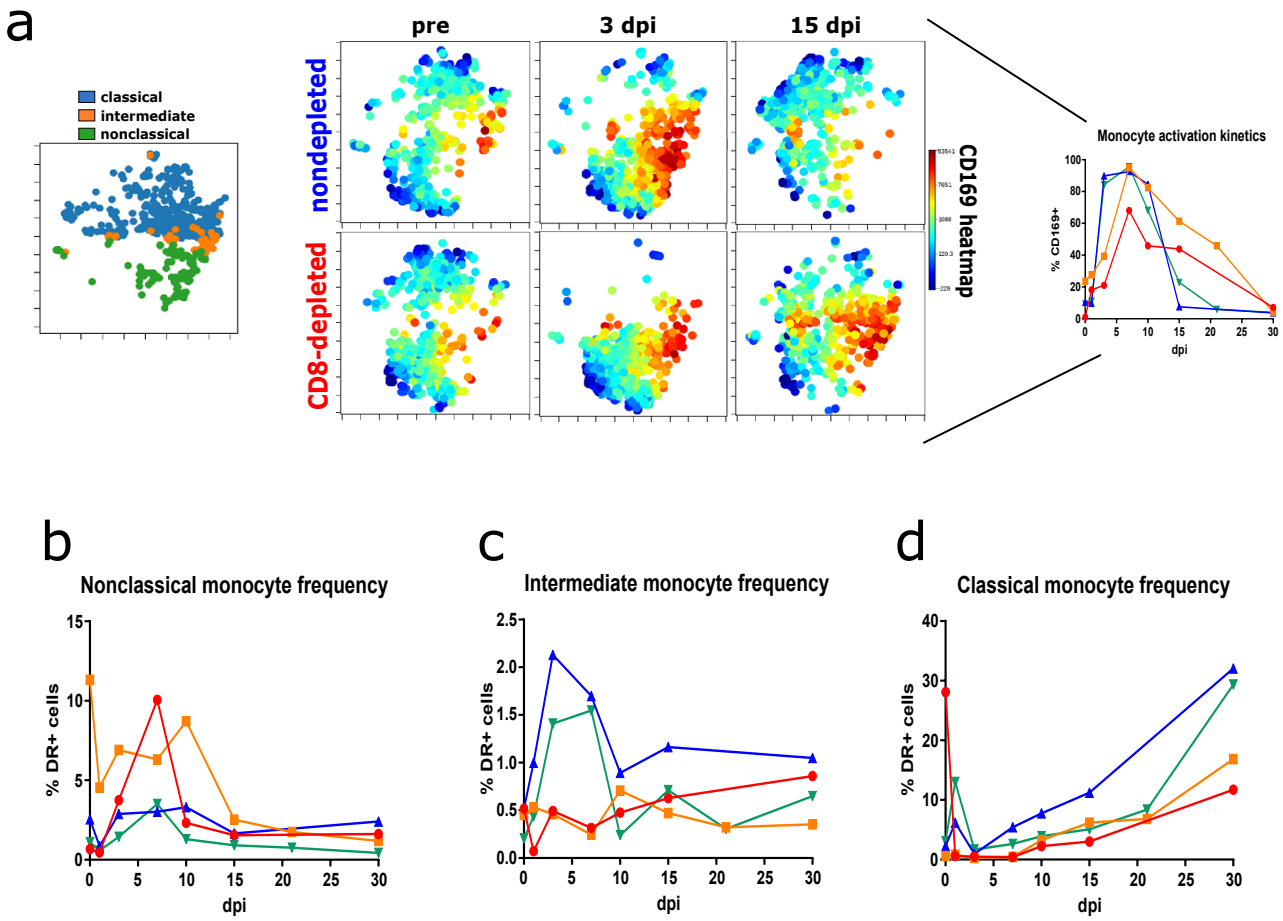

Fig 4: Possible compensatory CD4 and humoral responses in CD8-depleted macaques

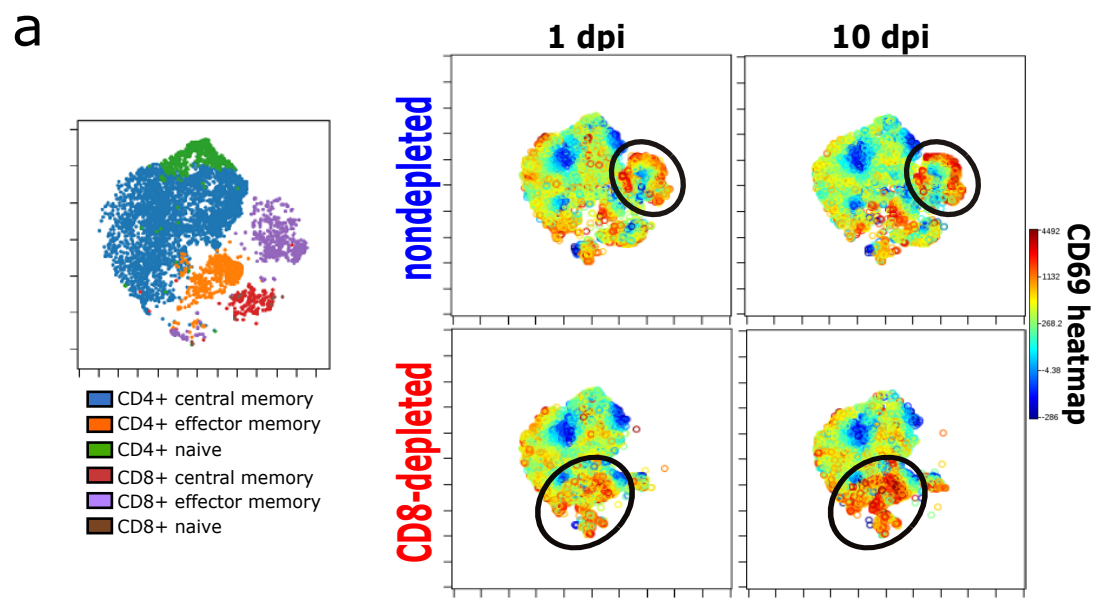

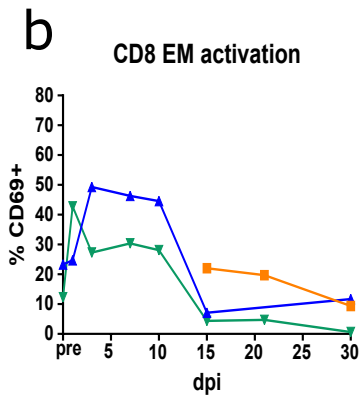

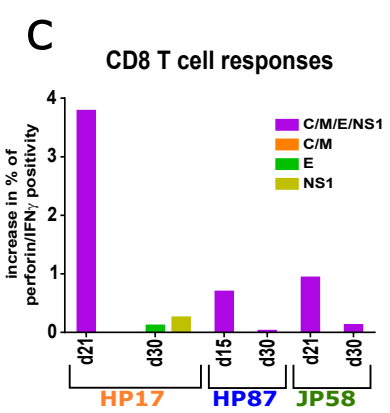

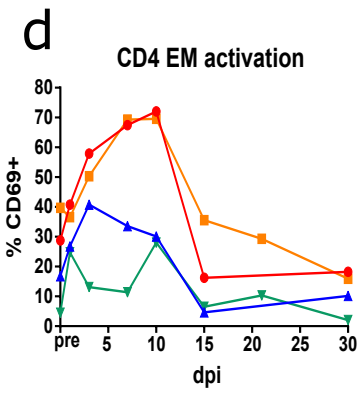

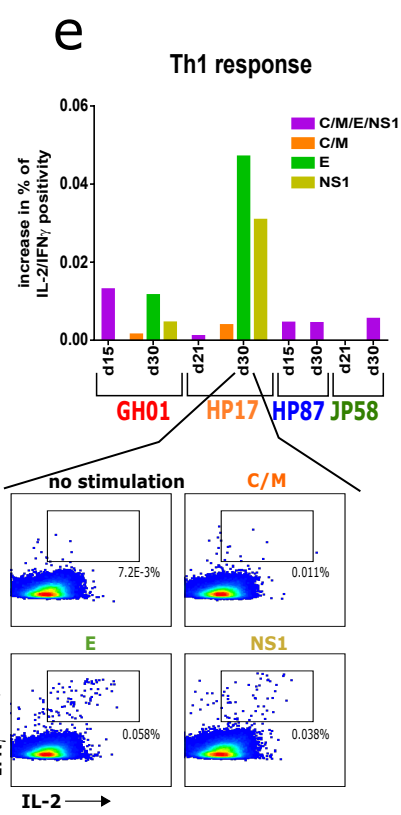

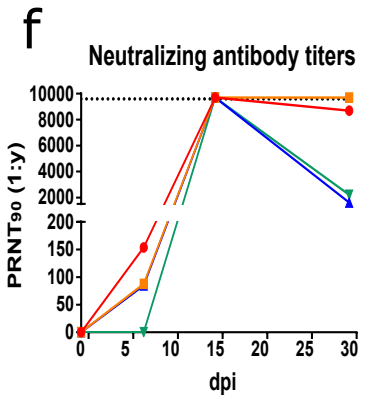

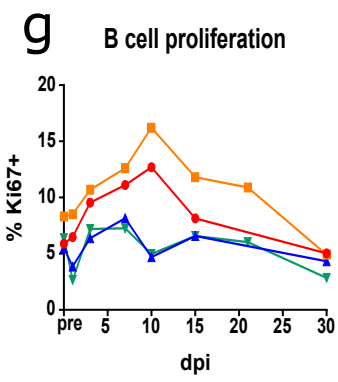

Fig 5: Enhanced viral dissemination and neuropathology in CD8-depleted macaques